Cement & Concrete Composites 32 (2010) 514–522

Contents lists available at ScienceDirect

Cement & Concrete Composites

journal homepage: www.elsevier.com/locate/cemconcomp

Pore space analysis of cement-based materials by combined Nitrogen sorption – Wood's metal impregnation and multi-cycle mercury intrusion

Josef Kaufmann *

Empa, Swiss Federal Laboratories for Materials Testing and Research, Überlandstrasse 129, Dübendorf, Switzerland

ARTICLE INFO

Article history:
Received 5 February 2010
Received in revised form 16 April 2010
Accepted 22 April 2010
Available online 28 April 2010

Keywords:
Pore size distribution
Mercury porosimetry
Nitrogen adsorption
Cement paste
Wood's metal impregnation

ABSTRACT

The analysis of pore space is crucial for a profound understanding of transport and mechanical properties of porous materials. Cement-based materials have a broad pore size distribution ranging from micro- to macro-pores. The analysis of this kind of pore space therefore becomes difficult. Because the resolution of image based methods is limited, indirect analysis methods like Nitrogen sorption or mercury intrusion porosimetry (MIP) are often applied. The standard MIP results in an underestimation of large pores because of its intrinsic limitation due to ink-bottle type pores (i.e., pores that are connected to the surface by smaller neck entrances only). The adsorption of Nitrogen seems to be less influenced by such connectivity effects, but the analysis of pores larger than about 100 nm is not possible.

To overcome these limitations, in this study pores were selectively filled with Wood's metal. The liquid metal (at elevated temperature) is intruded into the samples by applying different pressure regimes and then re-solidified in place. The partial impregnation with this metal allowed the analysis of non-ink-bottle type pore space in a subsequent Nitrogen sorption experiment and its comparison with an empty pore system. Furthermore, Mercury intrusion experiments with an additional pressurization–depressurization cycles (multi-cycle-MIP) were performed. The pore size distributions and pore volumes as calculated from Nitrogen sorption data are then compared with MIP and multi-cycle MIP data.

1. Introduction

Cement-based materials are porous, and the analysis of the pore space and its size distribution is crucial for a profound understanding of transport phenomena, mechanical properties and durability. While the total porosity may be sufficient to predict some macroscopic material properties, the analysis of the distribution of pore sizes and the connectivity of the pore structure is necessary for a deeper micro-structural understanding and the prediction of liquid or gas transport, creep, shrinkage and frost resistance.

Porosity and pore size distributions may be analyzed directly by image analysis techniques [1] or tomography methods [2]. Recently the development of 3D reconstruction methods based on focussed ion beam milling led to a spatial resolution of better than 30 nm [3,4]. However, a higher resolution often implies the drawback of smaller sample volumes.

Many indirect methods, among them sorption isotherms and mercury intrusion porosimetry (MIP) have been developed. Each of these has specific advantages and drawbacks. Nitrogen sorption and mercury intrusion porosimetry (MIP) allow the analysis of larger sample volumes and require less sophisticated equipment. These methods were selected for this study. The specific disadvantage of MIP is the well-known ink-bottle effect [5]. Larger pores that are only accessible by smaller neck entrances will be underestimated in size and lead to hysteresis effects. In this study it is shown that, by applying a second mercury intrusion cycle (multi-cycle-MIP) it is possible to overcome some of these problems.

Nitrogen sorption does, at least in adsorption, not suffer from such effects, but the analysis of larger pores (radius > 50 nm) suffers from poor resolution. Neck pores influence the desorption branch and lead to hysteresis effects as well [6]. In this study the effect of a partial impregnation of the pore system with Wood's metal prior to measurement [7] was studied. Wood's metal is intruded above its melting temperature and under well defined pressure into the samples and is then allowed to solidify by lowering the temperature. In this way, the large pores and/or the ink-bottle type pores may be selectively filled with this metal, so that they are excluded from analysis. The empty pore space is then characterized by Nitrogen adsorption. In this way the small-sized, but probably connected pores are analyzed. The results are then compared with the ones obtained from multi-cycle MIP experiments.

* Tel.: +41 44 823 4095; fax: +41 44 823 4035.
E-mail address: Josef.kaufmann@empa.ch

0958-9465/$ - see front matter © 2010 Elsevier Ltd. All rights reserved.
doi:10.1016/j.cemconcomp.2010.04.003

Table 1
Mixture design (quantities used to obtain 1 m^3 of cement-based material).

	Cement (kg/m^3)	Limestone filler (kg/m^3)	Water (kg/m^3)	Sand (kg/m^3)	HRWRA (kg/m^3)	w/c (w/p)	Paste volume (m^3/m^3)
Z	1398		559	–	–	0.40	1
M1	493	223	258	1320	4.8	0.52 (0.36)	0.42 (0.50[a])
M2	511	–	256	1534	–	0.50	0.42

[a] Including limestone filler.

2. Materials and methods

2.1. Materials and mix design

The mixture designs of the samples used in this study are given in Table 1. The whole experimental program is outlined in Fig. 1. An ordinary Portland cement CEM I 42.5 N according to European Standard EN 197-1 with a specific surface of 2900 cm^2/g (Blaine method) and a density of 3.17 g/cm^3 was used. The limestone filler that was used in mixture M1 had a similar grain size distribution as

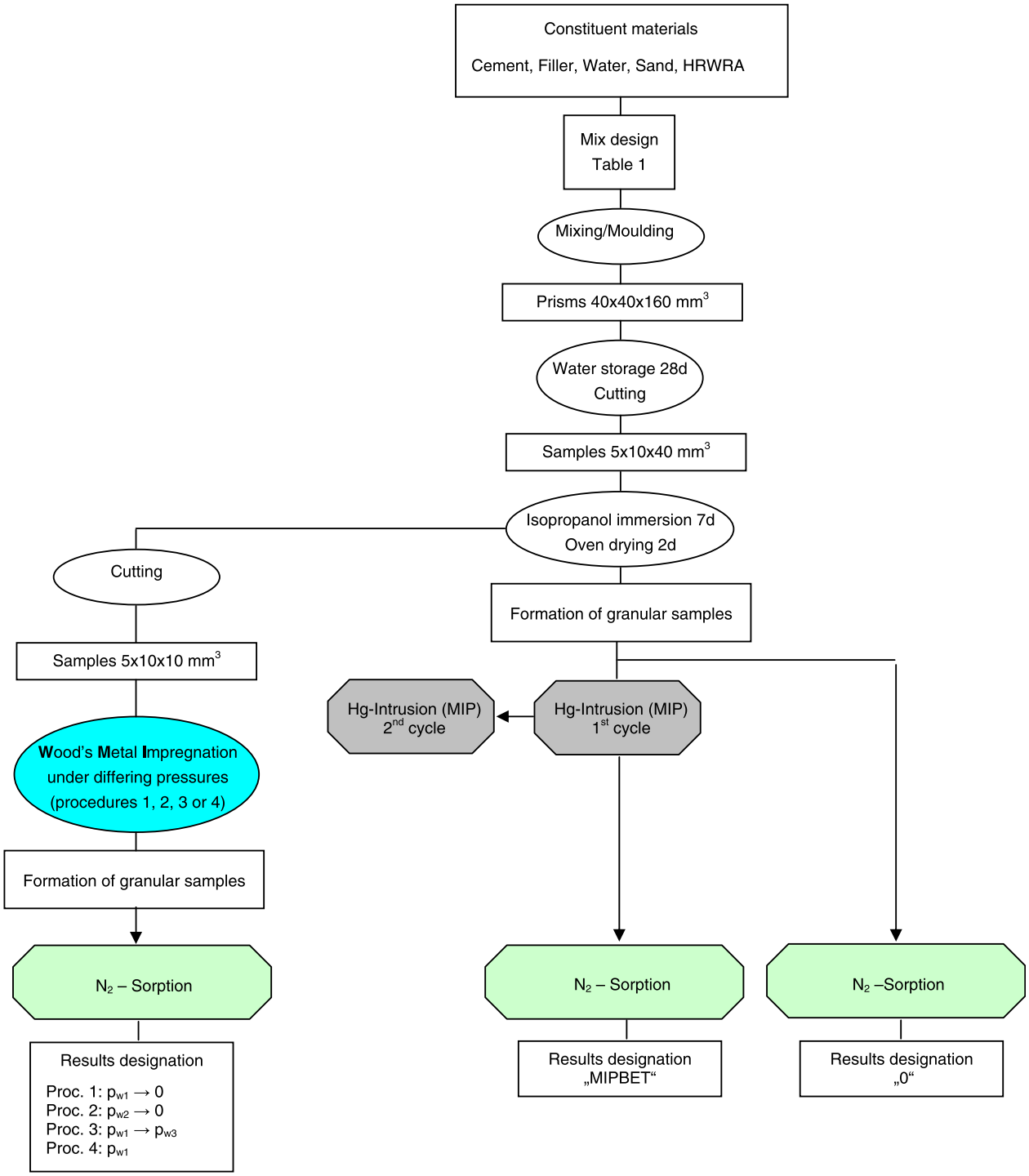

Fig. 1. Sequence of sample preparation and experimental procedures.

the cement and a density of 2.77 g/cm^3. Standard quartz sand 0–2 mm according to European Standard EN 196-1 with a density of 2.63 g/cm^3 was used as aggregate. A high range water reducer (HRWRA) based on polycarboxylate ether was applied in some cases. Mixture Z is a pure cement paste without sand addition. M1 is designed as self compacting mortar with limestone addition. Mortar M2 is a standard mortar according to European Standard EN 196-1. The cement content of M1 was chosen in a way that the cement to water ratio by volume was similar to the one of the standard mortar M2. A mixer according to EN 196-1 at stage I (62.5 rpm) was used to prepare the fresh mortars or pastes. Cement and sand were mixed for 1 min. The mixing water was added progressively during the next 30 s. After continuing the mixing for 90 s it was stopped for 15 s in order to scrape off the material that had adhered to the sides of the mixing bowl with a plastic spatula. After that, the mixing was continued for 90 s. Then prisms of $40 \times 40 \times 160$ mm^3 were produced and subsequently stored in water. At an age of 28 days, samples of about $5 \times 10 \times 40$ mm^3 were cut at the centre of the prisms and then immersed during 1 week into isopropanol for water exchange. These samples were then oven-dried at 50 °C during 2 days. The drying regime significantly influences the Nitrogen sorption as well as the metal intrusion results [8,9]. In this study, absolute dry levels are less important than the fact that the studied pore systems all were at the same initial dry level prior to measurements. Finally, small pieces with diameters of about 2 mm were broken for the different analyses.

Because the size of the sand used in the mortar mixtures is in the range of this size as well, these pieces are not large enough to have a representative elementary volume. However, experimentally it was not possible to use much larger pieces. In order to partly overcome the problem of representative volume, a multitude of such pieces were assembled to form one sample which then was measured. For one mercury intrusion measurement about 1.5–2 g of sample was used, which corresponds to more than 100 of such pieces. In Nitrogen sorption experiments about 0.5 g of pure cement paste (about 30 such pieces) or about 1.5 g of mortar were used. No selection of pieces was made, so that the analysis included the small aggregates (<2 mm) in the case of mortars. Some analyses were repeated and a very good reproducibility (deviation of the measured value at a certain pore size was less than 5%) was found in both experiments for all material types.

2.2. Wood's metal impregnation (WMI)

Dried samples were impregnated with Wood's metal (50% Bi; 26.7% Pb; 13.3% Sn; 10% Cd) in a specially designed pressure cell (see Fig. 2). As its melting point of 343 K is relatively low, this metal can be liquefied/solidified easily. Liquid Wood's metal is a non-wetting fluid which penetrates the pores of a material just under pressure. The Washburn equation [10] may be used to describe the relation between the applied pressure p and the radius r of the pores that are filled.

$$r = -\frac{\mathrm{F}\,\gamma\cos\Theta}{p} \tag{1}$$

where p: pressure, Θ: contact angle, γ: surface tension and F: form factor (=2 for cylindrical pores).

Abell et al. [11] observed contact angles of Wood's metal on mortar surfaces and found the observed values of 133–140° to be in the same range as values widely accepted for mercury. Darot and Reuschle [12] determined the product $\gamma \cos \Theta$ on quartz and found values in the range of 0.42–0.47 N/m which were higher than the ones obtained for mercury (0.327–0.386 N/m). In this study a value of $\gamma \cos \Theta$ = 0.42 N/m was used for pore radius calculations in the Wood's metal impregnation experiments. This is a higher value than the one applied to mercury intrusion experiments (0.367 N/m).

To impregnate the samples, the metal first was heated to liquefy. Then a certain well defined pressure level was applied to fill the pores that are larger than the corresponding radius. To make the impregnation permanent, the temperature was lowered maintaining the pressure level, to allow the Wood's metal to solidify.

A sample of about $5 \times 10 \times 10$ mm^3 was glued on the bottom of a cell, which then was filled with solid metal pieces. The cell was then heated to 85 °C under vacuum (<0.01 mbar) and closed by a piston. O-rings that are connecting the piston to the cell wall are able to bear pressures of more than 6000 bar.

Once the metal was liquid, a load by means of a press in controlled load mode was applied to the piston. Pressure increase in the cell was 7 MPa/min until maximum pressure $p_{w,max}$ was reached. The maximum pressure then was kept constant for 15 min. After that, the temperature was decreased at a cooling rate of about 1 K/min to solidify Wood's metal again. In other cases the load previously was reduced to a certain final pressure $p_{w,final}$ at a rate of 18 MPa/min and then kept constant for another 15 min. The temperature was not lowered afore. The load was regulated at all time to maintain the desired pressure level. This is extremely important as the thermal contraction (0.0001 K^{-1}) and the intrusion of the Wood's metal otherwise would lead to unknown pressure states and, due to shrinkage of the Wood's metal upon solidification, to badly defined impregnation.

The metal impregnated sample was then taken out of the cell, and the Wood's metal surrounding was removed by sawing, so that finally all sample surfaces were free of Wood's metal, which hence just remained present in their interior.

In this study two different maximum pressures were used: p_{w1} = 154 MPa ($r_{w1} \approx 5$ nm) and p_{w2} = 31 MPa ($r_{w2} \approx 27$ nm). The final pressure $p_{w,final}$ was either p_{w1} (almost full impregnation with Wood's metal), p_{w3} = 6 MPa ($r_{w3} \approx 140$ nm) or atmospheric pressure (denominated as "0"). As observed by scanning electron microscopy, even at the highest pressure, no crack formation caused by this impregnation was found.

In a simplified pore model consisting of large chambers that are interconnected by smaller necks and assuming snap-off of the metal meniscus upon pressure reduction (extrusion) only occurring at the intersection between the large chambers and the necks,

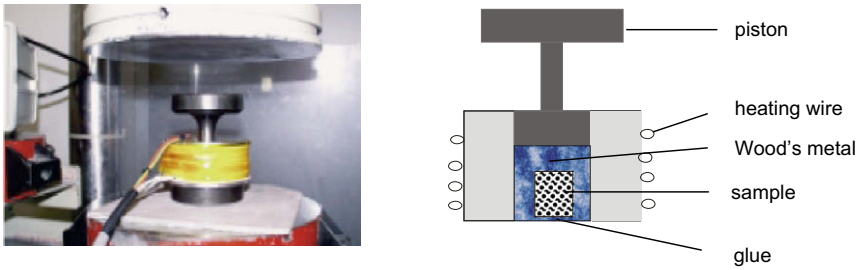

Fig. 2. Wood's metal intrusion apparatus.

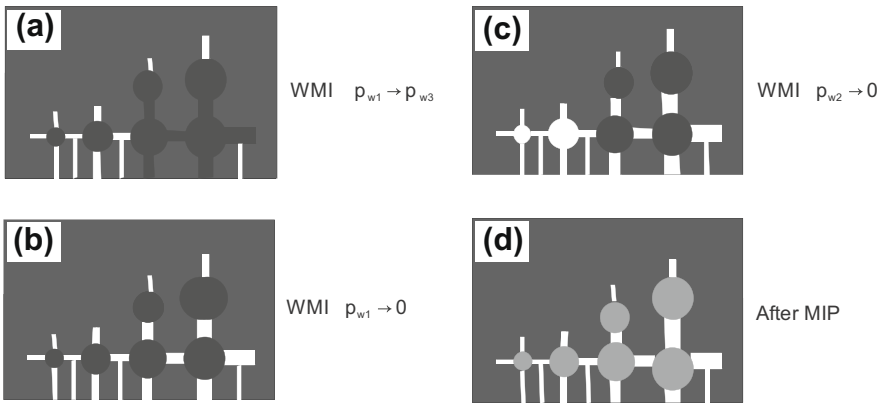

Fig. 3. Conditions in a pore system after Wood's metal impregnation and after a completed mercury intrusion porosimetry cycle (Wood's metal: dark, mercury: light grey).

impregnation levels as described schematically in Fig. 3 would result. When applying the high maximum pressure (p_{w1}) and a certain limited final pressure (p_{w3}) the Wood's metal is supposed to fill almost all ink-bottle pores and the coarser capillary pores after impregnation (Fig. 3a). When the final pressure is equal to the atmospheric pressure, only the ink-bottle pores will be impregnated (Fig. 3b). When a lower maximum pressure is applied (p_{w2}), only the ink-bottle pores with coarser necks will be filled with Wood's metal and remain impregnated after pressure release to atmospheric pressure and solidification of the metal (Fig. 3c).

2.3. Nitrogen sorption

Oven dried and Wood's metal impregnated specimens (as described above) were crimped to pieces of about 2 mm edge length. More than 30 pieces (mortar: 100 pieces) were put together in a glass vessel and analyzed as one sample. Some samples were studied after performing a full mercury intrusion cycle so that they were partly filled with mercury (Fig. 3d, denominated "MIPBET"). Nitrogen sorption analysis was performed on a Beckman Coulter SA 3100. Adsorption and desorption isotherms were measured.

The connectivity of the pore network plays an important role in determining the extent of a hysteresis. A simple example may explain the differences between adsorption and desorption. A small network of three pores U, V, W is considered (Fig. 4). The connection to the surface is through pore V only. As the pressure is increased during the adsorption process, the Nitrogen condenses in order of increasing pore size, i.e. in the sequence U → V → W. During desorption, the Nitrogen becomes thermodynamically unstable with respect to the vapor phase in the order W, V, U but the Nitrogen in the pore W is not in contact with the vapour phase and metastable Nitrogen persists until the Nitrogen in pore V, which is in contact to the vapour phase, vaporises. The order of vaporisation in desorption hence is V and W together, followed by U. The delay of vaporisation of pore W leads to a hysteresis. In a real pore system the situation gets much more complicated. However, assuming that filling time is not important and equilibrium is achieved in the experiment, filling (adsorption) will be from the finer to the larger pores, meanwhile in a real pore system the desorption process is rather complicated and metastable Nitrogen very common.

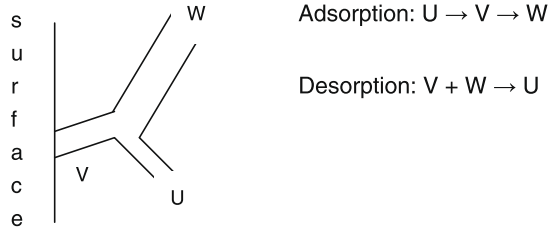

Fig. 4. Schematically filling and emptying of pores by Nitrogen [6].

2.4. Mercury intrusion porosimetry (MIP)

Specimens with the same drying level and dimensions as for nitrogen sorption analysis were studied. The analyses were performed using a Thermoelectron Pascal 140/440 equipment. Maximum pressure was p_{max} = 395 MPa. In general, raw data from mercury porosimetry is analyzed using the Washburn equation [10]. Assuming a contact angle of 140 ° and a surface tension of mercury of 0.48 N/m ($\gamma \cos \Theta$ = 0.367 N/m) this maximum pressure corresponds to a pore radius of 2 nm.

However it is well known that surface tension and contact angle both vary with the radius of curvature of the meniscus and hence upon whether the meniscus is advancing or receding.

This may be corrected assuming different contact angle for intrusion and extrusion [13,14]. A shift of the applied contact angle rescales the pore sizes by $\cos \theta_{instrusion} / \cos \theta_{extrusion}$. A constant change in contact angle by a factor of 2.657 [15] (from 140°/intrusion to about 107°/extrusion) leads to smaller calculated pore sizes in extrusion.

Instead of applying Washburn equation, Rigby and Fletcher [16] proposes a semi-empirical relation between pore radius r and applied mercury pressure p:

$$r = \frac{-A + \sqrt{(A^2 - 2pB)}}{p} \tag{2}$$

Owing to a lack of similar calculation for cement-based materials the values for silica as given in Table 2 may be used for the parameters A and B.

In order to reduce ink-bottle effects one may apply multi-cycle MIP. After a first complete intrusion/extrusion cycle a second complete cycle is added. Based on the assumption that in this way ink-bottle pores remain mercury filled after the first cycle

Table 2
Parameters for the insertion in Eq. (2) for silica [16].

	$A \times 10^3/(\mathrm{N\,m^{-1}})$	$B \times 10^{12}/(\mathrm{N})$	Range of validity radius r (nm)
Advancing meniscus	−302.5	−0.75	6–100
Retreating meniscus	−68.5	−235.5	4–70

(Fig. 3d), reduced hysteresis and no additional remaining mercury after extrusion is expected in the second cycle. However, the remaining mercury in the ink-bottle pores is liquid and such pores hence provide an inner surface from which the mercury penetration may proceed. This may influence the observed pore size distribution. The size of the ink-bottle pores is excluded from analysis in such multi-cycle MIP analysis, whereas an estimation of the sizes of their neck entrances is possible [15].

3. Results

3.1. Nitrogen sorption

The Wood's metal filling level significantly influences the Nitrogen isotherms (Fig. 5). The maximal amount of adsorbed Nitrogen ($p/p_0 \approx 1$) as well as the calculated BET surface area are highest for the empty sample and decrease with increasing Wood's metal intrusion pressure (Table 3). The maximum adsorbed Nitrogen volume of the studied batches scale rather well with the paste volume of the studied mixtures (including the limestone filler of batch M1 in volume calculations). The calculated BET surface of the mortars M1 and M2 scale well with their powder content (cement plus limestone filler), whereas this does not apply to the pure paste (Z), reflecting its lower w/c ratio. The impregnation with Wood's metal highest pressure level (WMI $p_{w1} \rightarrow 0$) and the impregnation with mercury ("MIPBET") lead to rather similar maximal Nitrogen adsorption for cement paste Z and mortar M1, meanwhile lower values for mercury impregnated samples are found for mortar M2. The reason for this may be the low powder content of batch M2 leading to a less connected pore system. Comparing the Wood's metal impregnation $p_{w1} \rightarrow 0$ with "MIPBET", equal impregnation level should result as both metals (liquid) possess similar physical properties.

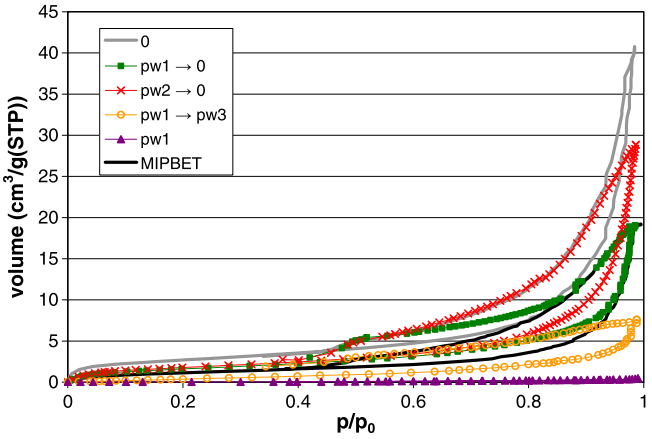

Fig. 5. Nitrogen sorption isotherms (adsorption branches are below desorption branches) for batch Z with different impregnation levels.

Table 3
BET surface (cm^2/g)//maximum N_2-volume absorbed (cm^3/g) at $p/p_0 \approx 1$.

Batch	Sample preconditioning			
	0	WMI: $p_{w1} \rightarrow 0$	WMI: $p_{w2} \rightarrow 0$	MIP: $p_{max} \rightarrow 0$
Z	9.81//40.79	6.17//19.06	6.85//28.84	4.54//19.21
M1	7.11//19.33	3.60//8.48	5.33//13.59	3.80//8.95
M2	5.17//15.58	2.01//6.78	3.20//11.1	1.12//4.55

For the cement paste Z some deviations in the small pore range result, whereas the total amount is equal. The differences may result from the fact that the Wood's metal gets solid after filling, whereas the mercury remains liquid. As the Nitrogen adsorption experiment is performed under vacuum and at very low temperatures, mercury redistribution cannot be excluded. Some smaller metal entrapped pores may be emptied under such conditions. This may explain the somewhat better agreement of the relative Nitrogen adsorption curves of WMI $p_{w2} \rightarrow 0$ with "MIPBET".

The filling level $p_{w1} \rightarrow p_{w3}$ leads to a much lower Nitrogen adsorption level. One has to take into account that the blockage of the pores with Wood's metal is upon extrusion. Assuming a similar contact angle correction for the retracting Wood's metal meniscus as for a mercury meniscus, the corresponding blockage radius r_{w3} would be much smaller ($r_{w3,retracting} = r_{w3}/2.657 \approx 53$ nm) and hence more pore space is blocked after Wood's metal impregnation.

As expected, a full Wood's metal impregnation of the sample at p_{w1} leads to very low Nitrogen adsorption.

For a further analysis, the observed Nitrogen isotherms are normalized setting the measured Nitrogen volume at $p/p_0 = 0.98$–100% (see Figs. 6 and 7). The normalized adsorption isotherms for sample Z reveals that the relative Nitrogen adsorption is (unlike the total amount and the absolute distribution) hardly influenced by the impregnation level. This indicates that the pore size distribution of the (after metal impregnation) remaining accessible empty pores, at least the pores that get filled with Nitrogen (e.g. the fine pores with radius < 50 nm), is rather similar to the one of an empty sample.

Only the full impregnation with Wood's metal (intrusion and hardening of Wood's metal at p_{w1}) leads to significant differences.

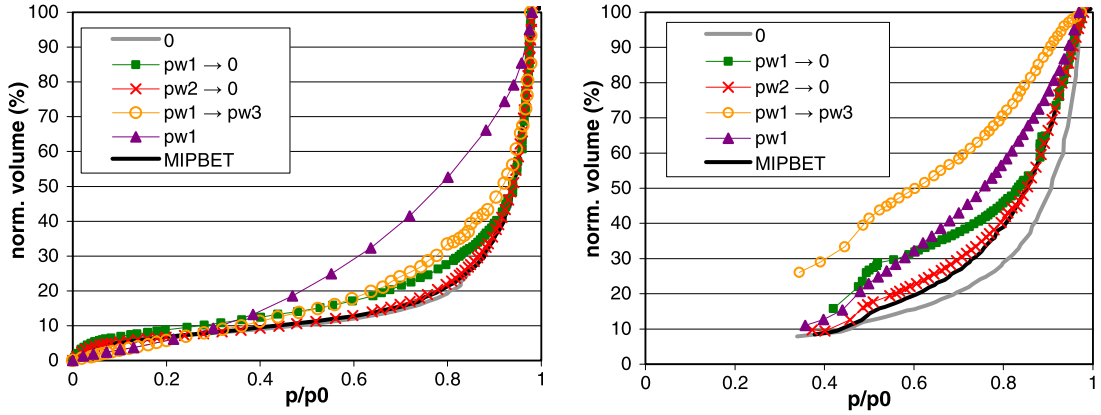

Fig. 6. Nitrogen volume normalized at $p/p_0 = 0.98$ for mixture Z. Left: adsorption, right: desorption.

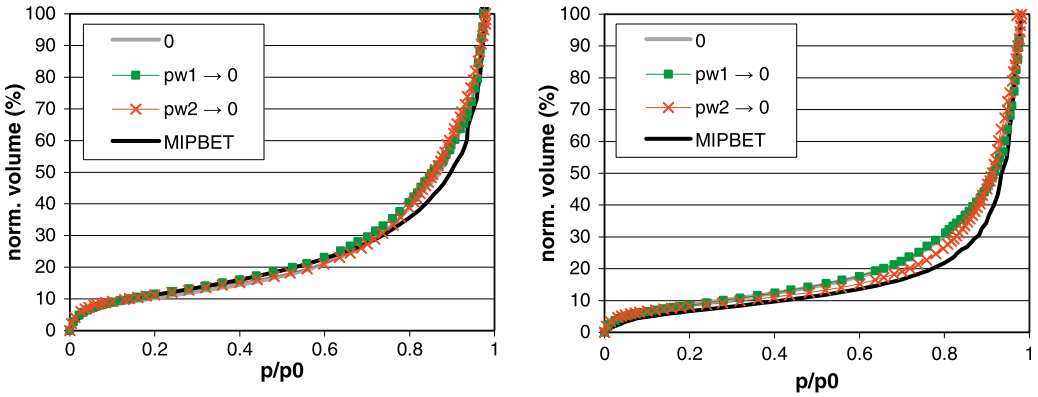

Fig. 7. Nitrogen adsorption volume for mixture M1 (left) and mixture M2 (right) normalized at $p/p_0 = 0.98$.

On the other hand, the desorption isotherms vary significantly with the impregnation level of the samples. This may be attributed to metastable Nitrogen in non-connected pores (see Fig. 4). As the connectivity of the pore space may be significantly changed by the blockage of certain pores with Wood's metal (or mercury), the distribution of metastable Nitrogen is altered and hence the desorption branch is different for different impregnation levels.

Nitrogen adsorption data for batches M1 and M2 is given in Fig. 6. The differences in the adsorption curves of different impregnation levels are very small either, confirming the conclusions derived from the experiments with pure cement paste.

Pore size distributions as calculated from adsorption or desorption branch applying BJH theory [17] for non-metal impregnated samples are plotted in Fig. 8. A small hysteresis between adsorption and desorption is observed. The desorption branch is shifted towards smaller sizes.

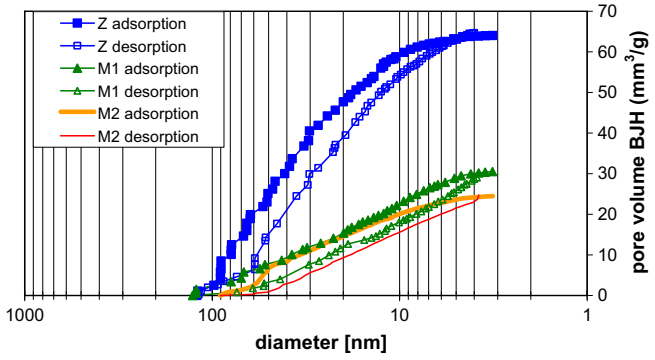

Fig. 8. Pore size distributions as calculated from Nitrogen sorption isotherms applying BJH theory.

3.2. Mercury intrusion porosimetry

After a first complete mercury intrusion cycle, a significant amount of mercury remains within the samples (Fig. 9, left). This may be attributed to a large ink bottle pore volume of nearly 50% of the whole porosity. The intrusion curve (1st intrusion) hence is not representing a realistic pore size distribution [5].

It is now assumed that after the first MIP cycle, the ink bottle pore space remains filled with entrapped mercury. If this would be the case, the ink-bottle pores do not have to be filled with mercury in a second MIP cycle. However, these pores then may serve as intrusion sites acting like an inner surface from which the mercury penetrates. The result of such a second MIP cycle is shown in Fig. 9 (right).

The hysteresis in the second cycle persists. However this hysteresis may be attributed to the fact that the surface tension, contact angle or form factors vary whether the meniscus is advancing or receding. A recalculation of pore size according Rigby and Fletcher [16] and a simple contact angle recalculation for the extrusion branch are shown in Fig. 10. However, when applying a correction according [16] (Fig. 10 left) the volume of pores with diameter smaller than about 10 nm calculated from the extrusion branches is shifted to smaller diameters. Applying a simple contact angle correction (Fig. 10 right) intrusion and extrusion curves cross each other at a diameter of about 10 nm.

The corrections for advancing and retracting meniscus lead to very good agreement between intrusion and extrusion in MIP

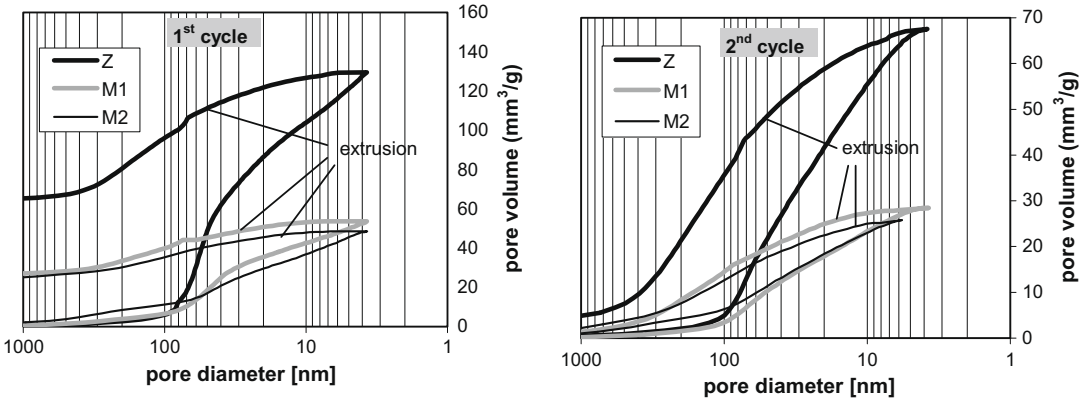

Fig. 9. MIP 1st and 2nd cycle – pore size calculation with Washburn equation (note the different scales).

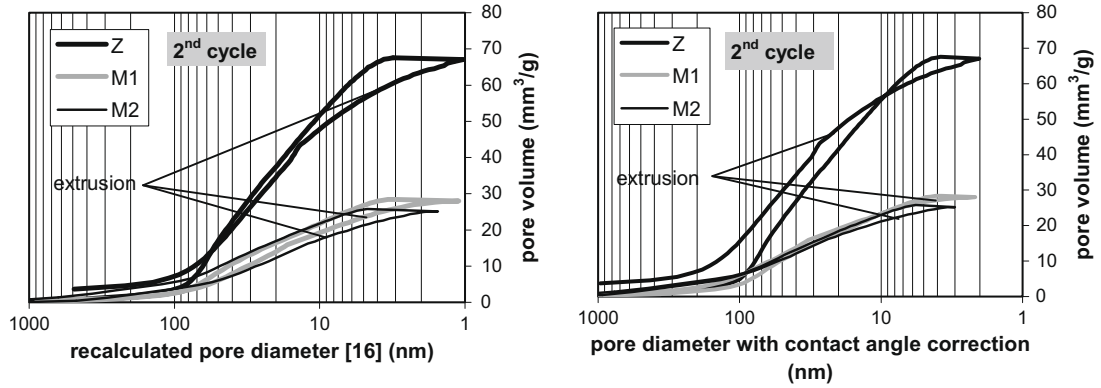

Fig. 10. Alternative pore size calculation: left – according to Rigby and Fletcher [16], right – contact angle correction.

experiments and hence support the assumption that the hysteresis in the second MIP cycle indeed may be explained by a different surface wetting of the mercury in extrusion compared with intrusion.

4. Discussion

4.1. Pore blocking by metal trapping

In a first approach (Fig. 3) it was assumed that the cement pore system consists of large chambers connected by smaller necks. Furthermore, it was assumed that upon retraction snap-off of the meniscus at the neck–chamber interface occurs, so that the chambers (large ink-bottle pores) remain selectively filled with metal, leaving empty pore necks that can be subsequently assessed by Nitrogen sorption.

Hence it is important to have a closer look at the cementitious pore system and its possible impact on metal trapping and the subsequent Nitrogen adsorption. The hydrated cement paste contains capillary pores with a big variation in size and geometry originally resulting from the cement particle spacing in the cement water suspension, and smaller pores which are the interlayer in the calciumsilicatehydrate (C-S-H) or other hydrate products [18]. Around the aggregates (mortar, concrete) a porous interfacial transition zone is present [1,19]. The sizes of the capillary pores may be assumed to be of mesoporous to macroporous range whereas the interlayer pores are assumed to have sizes of about 1–3 nm [20]. As the interlayer-pores are formed around all cement particles upon ongoing hydration, it may be a reasonable assumption that they form a kind of small-sized sub-pore network interconnecting all the other (larger) pores. Scanning electron images of ordinary Portland cement pastes (see Fig. 11 – segmented according the grey scale level) reveal relatively large isolated pores which perfectly may be described as ink-bottle pores. The interconnecting smaller pores are not sufficiently resolved in such images.

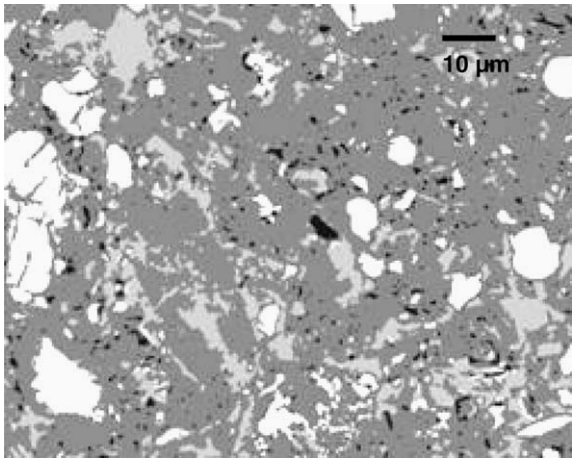

Fig. 11. Segmented SEM image of OPC paste at 28d (black = pores).

A real pore system, especially a cementitious one, hence is much more complicated than a simplified neck/chamber system including complex geometries and different sizes.

Furthermore, metal trapping is a complicated process and may result in partial filling of different pore space and different filling levels from what is shown in the simplified Fig. 3. Many experiments and theoretical simulations have shown that even in a simplified neck chamber system both necks and chambers may remain filled or partially filled following the release of pressure [21]. Studying relatively coarse pore systems, Wardlaw and McKellar [22] finds trapping of mercury during withdrawal to be influenced by pore to neck size ratio, coordination number and non-random heterogeneities also.

However, the Nitrogen may not detect inner pores that have been blocked off by trapped metal and it would only measure the empty or partially filled pores (necks and chambers) that are accessible from the surface.

4.2. Accessibility of metal blocked pores

The experiment shows that the metal impregnation level has only a minor influence on the relative Nitrogen adsorption and hence on the pore size distribution of the Nitrogen accessible pore space (Figs. 6 and 7). The partly metal impregnated system (at least WMI $p_{w2} \rightarrow 0$ and after a first mercury intrusion cycle) reveals a very similar relative Nitrogen adsorption behavior as the empty pore system (“0”). However, the absolute value of adsorption for all Nitrogen pressures depends strongly on the metal impregnation level (Fig. 5).

This may be explained in two different ways: (i) the trapped metal completely fills pores that are of similar sizes and distribution as the empty pore system or (ii) the solidified metal (or even the liquid mercury remaining in the system after extrusion) blocks whole partly empty pore regions, with similar pore size distributions as an empty system, from any Nitrogen access. These pores may remain partly empty after metal impregnation.

The first possibility seems to be very unlikely. In a pore system with a broad pore size distribution, the pressure differences become very high and selective blocking of certain specific pore sizes would be expected. The smallest pores are supposed to empty first upon metal pressure reduction [21,22].

Hence, situation (ii) seems to apply and the metal seems to block whole partly empty pore space from any Nitrogen access. Looking at the composition of the pore system of cement-based materials containing a sub-network of interlayer pores, it is somewhat astonishing that these small-sized pores should not access all empty pores to the provided Nitrogen at the sample surface. The dynamics of Nitrogen filling may play a role. These interlayer pores are very small in size and get filled quickly by surface adsorption at relatively low Nitrogen pressures. Contrary, Nitrogen transport through such pores may have rather slow kinetics, so that the time to reach Nitrogen equilibrium in larger pore areas that are only accessible through these pores, would be very long.

In a partially metal filled pore system of situation (ii) (like for instance after Wood's metal impregnation $p_{w2} \rightarrow 0$ or after a first mercury intrusion cycle) we generally can define three different pore type regions – F: metal filled pores – B: empty pores that could be filled by Nitrogen but are blocked from Nitrogen access (in experimental equilibrium time limit) by the metal – E: empty pores that are filled by the Nitrogen. Type E pore space was found to have the same pore size distribution (relative Nitrogen adsorption behavior) as the completely empty pore system. The type F pore space is likely to have a different (coarser) size distribution. Actually, in the Nitrogen adsorption experiment pores that have a radius larger than the detection limit of the Nitrogen adsorption measurement (about 50 nm at the applied maximal Nitrogen pressures and equilibrium time) remain empty, even when they are accessible to the Nitrogen at the surface. Let us assign this pore space as – L: large pores that are not analyzed in the Nitrogen sorption experiment.

The metal impregnated pore space F may be subdivided into pores – F_1: larger than Nitrogen detection limit and – F_2: smaller than Nitrogen detection limit.

4.3. Pore volume comparison

Let us now consider the situation when mercury is the trapping metal and compare two different experimental results. First we look at the situation in a second mercury intrusion experiment. After the first mercury cycle, metal is entrapped in the pore space $F_{mercury}$ (= $F_{1,mercury} + F_{2,mercury}$). In the second mercury intrusion cycle, at the maximal pressure (p_{max} = 395 MPa), all the empty pore space of type B, E and L (pores larger than $r_{p,max} \approx 2$ nm) get filled with mercury.

We now consider the Nitrogen adsorption experiment of empty, non-metal impregnated samples (result designation "0"). In the terminology defined above, the pore space B, E and F_2 (in this experiment they are not metal filled) is assumed to get filled with Nitrogen, that means all pores except the large pores (type L and F_1). The smallest pore sizes are assumed to be filled by surface adsorption and are not included in the pore volume calculations presented in Fig. 8 which only includes pores larger than 2 nm.

Comparing the total pore volume that is filled when mercury (2nd cycle) is intruded into the system (Fig. 9 right) with the Nitrogen pore volume (non-micro) of the completely empty sample (Fig. 8), rather similar amounts are observed (about 70 mm^3/g for Z, 30 mm^3/g for M1 and 25 mm^3/g for M2). The pore space B + E + L (2nd mercury) seems to have the same volume as the pore space B + E + F_2 (Nitrogen). From a difference calculation we hence conclude that the amount of pores of type F_2 (mercury filled after the first intrusion and "small" – Nitrogen measurable) is equal to the amount of pores of type L (empty after mercury impregnation, "large" – not Nitrogen measurable), which is a rather surprising result. This result is found for the different cementitious pore systems Z, M1 and M2. In a mortar system (M1 or M2), where coarser pore sizes around the interfacial transition zone may be expected, this relation should be different from the one of a pure cement paste.

A solution of this contradiction is the conclusion that neither F_2 type nor L type pores are present in the system. Alternatively, we can say that after completing the first mercury intrusion cycle all F-type (metal filled pores) are large, non-detectable pores in Nitrogen adsorption experiment and furthermore, that all large pores which are non-detectable by the Nitrogen adsorption remain metal filled. This is found without any further pore model or metal trapping mechanism assumptions. This supports the assumption that snap-off at the ink-bottle boundaries is supposed to be more important than snap-off of the mercury in a connected network. The assumption of large chambers interconnected by smaller necks which remain empty after liquid metal retraction seems to be reasonable. The volume of the ink-bottle pores hence can be calculated as the amount of remaining mercury after completing the first mercury intrusion cycle.

4.4. Accessibility considerations

Even in a neck-chamber model the accessibility of the chamber (and the pore space accessible only through such a chamber) would depend on the connectivity to the surface. The relative pore size distribution would not be influenced, in contrast to the absolute trapped metal or ink-bottle type pore space. In our experiments, small-sized samples have been used. Larger sizes or larger distances from an outer surface are supposed to have bigger influence on metal snap-off and filling behavior. The connectivity in cementitious systems with a high content of capillary pores is supposed to be better than in a relatively dense system. This may also be the case in mortar systems where the porous interfacial transition zone around the aggregates may serve as a sub-network increasing the accessibility. In less connected pore systems or at longer distance from the surface, the ink-bottle type pores may get smaller in size. This would imply that the detection of smaller ink-bottle pores in Nitrogen adsorption experiments may be possible, so that the amount of Nitrogen pore space would become larger than the one found in a multi-cycle mercury intrusion experiment. Corrections for Nitrogen filled ink-bottle type as proposed in [15] would be necessary, but the above conclusions still would be valid.

4.5. Pore size distribution comparisons

In the observed cement-based material systems we saw in Nitrogen sorption experiments that the relative Nitrogen adsorption volume and hence the pore size distribution of the pores that are not blocked from Nitrogen access through the metal impregnation is similar to the one of a completely empty sample. Furthermore, we may conclude from above considerations that the metal preferentially traps relatively large ink-bottle type pores. So the empty pore space blocked by the metal from Nitrogen access consists of small pores (within Nitrogen detection limit) only. Hence the blocked pores also should possess a similar pore size distribution as the none-blocked pores or the empty sample. We can conclude that in a second mercury cycle, the mercury that intrudes from the inner sites which remain mercury filled after the first cycle detects pores with the same size distribution as the ones accessed by the mercury from the outer sample surface. Furthermore, the Nitrogen adsorption experiment and the 2nd mercury intrusion should deliver similar pore size distributions. The results of the Nitrogen adsorption (Fig. 8) and the 2nd mercury intrusion (Fig. 9, right) in the observed cement-based material systems indeed deliver rather similar pore size distribution results and support the above conclusions.

A pore size analysis by multi-mercury intrusion as proposed in [15] hence seems to be reasonable. The remaining mercury after the first cycle is considered as the ink bottle volume. A subtraction of the volume data of a second intrusion cycle from the data of a first intrusion cycle delivers the mean sizes of neck entrances. Finally the pore size distribution calculated from the second mercury intrusion cycle represents the pore size distribution of the surface connected (not ink-bottle type) pores.

5. Summary and conclusions

The pore system of cement-based materials was studied by Nitrogen sorption and mercury intrusion porosimetry. The partial filling of a pore system with immobile Wood's metal changes the amount of the adsorbed Nitrogen and its absolute distribution, but did not alter the relative shape of the Nitrogen adsorption isotherms. The relative pore size distribution of the accessible pore space hence is not influenced by the metal impregnation of ink-bottle type or large pores and is similar to the one of an empty pore system.

The pore size distribution as derived from Nitrogen adsorption was compared with mercury intrusion. Multiple cycling was found to be a useful tool to characterize the pore sizes with mercury intrusion. Applying a second intrusion cycle a much smaller hysteresis between intrusion and extrusion was found, concluding that ink-bottle pores remain filled after the first cycle and hence do not influence the MIP result drastically any more. The non-ink bottle pore space may hence be analyzed in a more accurate manner.

The Nitrogen adsorption measurement leads to similar pore volume and pore size distribution as the multi-cycle mercury intrusion. The ink-bottle pores in the studied mortars and cement paste seem to consist of pores with a larger size (diameter > 100 nm) which are not analyzed in Nitrogen sorption analysis.

In comparison with Nitrogen sorption data, multi-cycle MIP still shows a relatively large hysteresis between intrusion and extrusion, which cannot be explained by ink bottle or neck pore effects. A simple contact angle reduction for the extrusion branches or the application of semi-empirical pore size pressure relations instead of Washburn equation reduces these hysteresis effects. The origin of this hysteresis in MIP experiments hence may lay in differences in surface tension, contact angle or shape between advancing and retracting mercury meniscus.

We may conclude that the pore volume and the distribution of the small pores (pores smaller than the detection limit of Nitrogen sorption) are analyzed best in a Nitrogen adsorption experiment. However, no information about pore connectivity is available in Nitrogen adsorption experiment. In a mercury intrusion experiment we can determine the amount of ink-bottle type pores. The size of the pores that are connected through larger pores to the surface can be determined when an additional second mercury intrusion cycle is performed.

The size distribution of ink-bottle type pores can neither be analyzed satisfactorily in multi-cycle mercury intrusion nor by Nitrogen adsorption experiments. However, the ink-bottle type pores in not very dense cement-based material systems such as the ones studied in this work (mortars and cement pastes with water/powder ratio > 0.4) were found to have diameters larger than 100 nm and hence image analysis based methods may complete the pore size analysis of cement-based materials.

References

[1] Scrivener K. Backscattered electron imaging of cementitious microstructues: understanding and quantification. Cem Concr Compos 2004;26:935–45.
[2] Monteiro P, Kirchheim A, Chae S, Fischer P, MacDowell AA, Schaible E, et al. Characterizing the nano and micro structure of concrete to improve its durability. Cem Concr Compos 2009;31:577–84.
[3] Holzer L, Indutnyi F, Gasser Ph, Münch B, Wegmann M. Three-dimensional analysis of porous $BaTiO_3$ ceramics using FIB nanotomography. J Micros 2004;216(1):84–95.
[4] Münch B, Holzer L. Contradicting geometrical concepts in pore size analysis attained with electron microscopy and mercury intrusion. J Am Ceram Soc 2008. doi:10.1111/j.1551-2916.2008.02736.x.
[5] Diamond S. Mercury porosimetry an inappropriate method for the measurement of pore size distributions in cement-based materials. Cem Concr Res 2000;30:1517–25.
[6] Seaton N. Determination of the connectivity of porous solids from nitrogen sorption measurements. Chem Eng Sci 1991;46:1895–909.
[7] Willis K, Abell A, Lange D. Image-based characterization of cement pore structure using Wood's metal intrusion. Cem Concr Res 1998;28:1695–705.
[8] Espinosa M, Franke L. Influence of the age and drying process on pore structure and sorption isotherms of hardened cement paste. Cem Concr Res 2006;36:1969–84.
[9] Gallé C. Effect of drying on cement-based materials pore structure as identified by mercury porosimetry-a comparative study between oven-, vacuum and freeze–drying. Cem Concr Res 2001;31:1467–77.
[10] Washburn EW. Note on a method of determining the distribution of pore sizes in porous materials. Proc Natl Acad Sci USA 1921;7:115–6.
[11] Abell A, Willis K, Lange D. Mercury intrusion porosimetry and image analysis of cement-based materials. J Colloid Interface Sci 1999;211:39–44.
[12] Darot M, Reuschle T. Wood's metal dynamic wettability on Quarz, granite and limestone. Pure Appl Geophys 2003;160:1415–27.
[13] Kloubek J. Hysteresis in porosimetry. Powder Technol 1981;29(1):63–73.
[14] Wardlaw N, Taylor R. Mercury capillary pressure curves and the interpretation of pore structure and capillary behaviour in reservoir rocks. Bull Can Pet Geol 1976;24(2):225–62.
[15] Kaufmann J, Loser R, Leemann A. Analysis of cement-bonded materials by multi-cycle mercury intrusion and nitrogen sorption. J Colloid Interface Sci 2009;336:730–7.
[16] Rigby S, Fletcher R. Interfacing mercury porosimetry with nitrogen sorption. Part Part Syst Char 2004;21:138–48.
[17] Barrett EJ, Joyner LG, Haleda PH. The determination of pore volume and area distributions in porous substances–I computations from nitrogen isotherms. J Am Chem Soc 1951;73:373–80.
[18] Jennings H. A model for the microstructure of calcium silicate hydrate in cement paste. Cem Concr Res 2000;30:101–16.
[19] Leemann A, Muench B, Gasser Ph, Holzer L. Influence of compaction on the interfacial transition zone and the permeability of concrete. Cem Concr Res 2006;36:1425–33.
[20] Mehta PK, Manmohan D. Pore size distribution and permeability of hardened cement pastes. In: Proc. 7th int. congr. on chemistry of cement, vol. III, Paris 1980, p. VII-1–5.
[21] Rigby S, Chigada P, Evbuomvan I, Chudek J, Miri T, Wood J, et al. Experimental and modelling studies of the kinetics of mercury retraction from highly confined geometries during porosimetry in the transport and the quasi-equilibrium regimes. Chem Eng Sci 2008;63:5771–88.
[22] Wardlaw N, McKellar M. Mercury porosimetry and the interpretation of pore geometry in sedimentary rocks and artificial models. Powder Technol 1981;29:127–43.